Coupled Simulation of the Injection and Combustion Process of an Industrial Diesel Engine

Daniel Jörss[1], Maximilian Ringel[1], Bert Buchholz[2], Christian Fink[1*]

[1]Department of Mechanical / Process and Environmental Engineering, Wismar University of Applied Sciences, Philipp-Müller-Str. 14, 23966 Wismar, Germany; *Christian.Fink@hs wismar.de*
[2]Chair of Piston Machines and Internal Combustion Engines, Rostock University, Albert-Einstein-Straße 2, 18059 Rostock, Germany

SNE 34(4), 2024, 195-202, DOI: 10.11128/sne.34.tn.10712
Selected ASIM WS 2023 Postconf. Publication: 2023-10-15
Rec. Improved English Vs.: 2024-08-06; Accepted: 2024-09-15
SNE - Simulation Notes Europe, ARGESIM Publisher Vienna
ISSN Print 2305-9974, Online 2306-0271, www.sne-journal.org

Abstract. In order to comply with future exhaust emission limits, very precise control of the injection quantity and injection timing is of crucial importance. The injection system fulfillling these requirements in the best way is the common rail system.
The model presented here describes a 1D hydraulic injector model in Simscape™, which is coupled to a zero-dimensional combustion engine model. Measurements were carried out using an injection rate analyser to validate the injector model. Good results were achieved between simulation and experiment.
In the second step, a model developed in Matlab® Simulink® [1] was extended with a phenomenological combustion model according to Barba [2]. The injection rate is transferred to the combustion model as an input parameter. This is used to calculate the heat release rate by means of the combustion engine model, taking other sub-models into account. Good agreements were achieved between the heat release rate calculated from the pressure curve analysis and the simulation.

Introduction

The introduction of common-rail injection technology has made it possible to decouple pressurisation and injection in terms of timing, pressure and number of injections. The necessary injection pressure in the system is generated by a separate high-pressure pump. The pressurised fuel is then accumulated in a high-pressure rail which is placed between the pump and the injectors. Instead of pressure-controlled injection nozzles, electrically actuated injectors are used in common-rail systems. The timing and duration of the injection is determined by the electrical control of the injector.

This allows for wide flexibilities with regard to multiple injection strategies and injection pressure depending on the load point. This makes it possible to develop injection strategies in such a way that considerable emission reductions can be achieved by engine internal measures.

The timing, the injection rate and the atomisation quality of the fuel injected into the combustion chamber prove to be important parameters. Extensive test bench trials are often necessary for the best possible adaptation of each operating point in the engine map. With today's simulation methods it is possible to model the complex processes in a combustion engine in detail to better understand the operating and emission behaviour and to analyse the effects of different applications.

This paper describes the model of a common-rail injector connected to a zero-dimensional combustion engine model [1] and compares the simulation results obtained with test bench measurements.

1 Model Description

The physical object-orientated toolbox Simscape™ was selected in Simulink® to simulate the common-rail injector. Conventional common-rail injectors consist of three main assemblies: the control valve, the injection nozzle and a mechanical-hydraulic coupling element. With reference to Figure 1, the pressure in the valve control chamber (2) determines whether the injection nozzle opens or closes or remains opened or closed. The magnitude of the pressure in the control chamber depends on the rail pressure on the one hand and the ratio of the inlet and outlet throttle on the other.

If the control valve is open, fuel flows out of the control chamber via the outlet throttle and the pressure drops.

A falling pressure reduces the force acting on the control piston on the nozzle needle, which is subjected to a force equilibrium. When the pressure falls below a certain level, the nozzle needle opens and the injection process begins. When the control valve closes the outlet throttle, the pressure in the control chamber rises and increases the force acting on the nozzle needle via the valve control piston until it closes and ends the injection process.

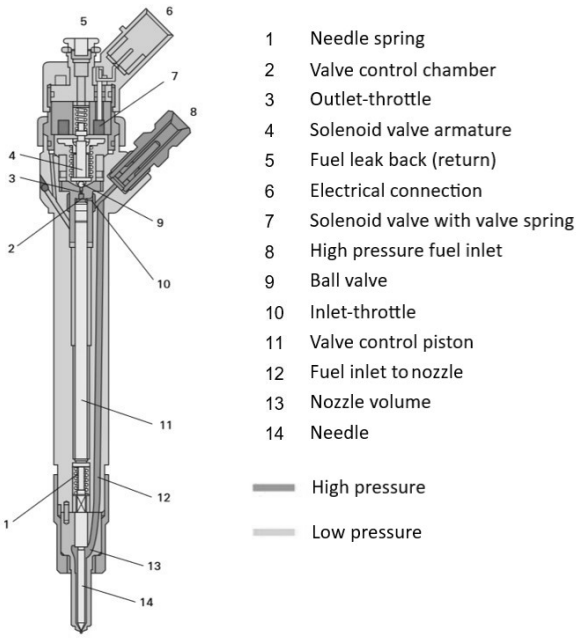

Figure 1: Structure of a typical solenoid valve injector [3].

In the simulation environment, the injector is divided into subsystems in which different domains of Simscape™ are used. The geometric dimensions of the individual components and the volume of the injector to be simulated were determined in advance by measurements. Parameters of the solenoid valve were taken from [4], [5].

1.1 Solenoid Valve Model

The solenoid valve model comprises a total of four domains from the Simscape™ library. Figure 2 shows how the individual blocks are connected to each other. The structure of this submodel includes a pulse width modulated voltage signal as input variable in accordance to [4]. Taking into account the ohmic resistance and the inductance, this results in the solenoid current.

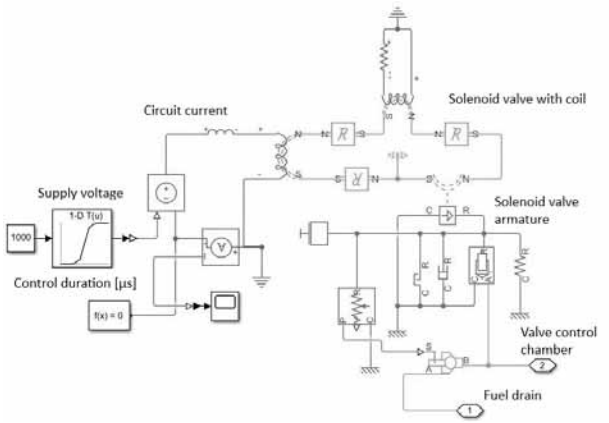

Figure 2: Structure of the solenoid valve in Simscape™.

The actuation time for the solenoid valve results from the time curve of this signal. This relationship is shown as an example in Figure 3 for a solenoid actuation duration of 1000 µs. The current creates a magnetic field in the coil of the solenoid valve, which attracts the solenoid valve armature. If the magnetic force outweighs the opposing spring force and the pressure force acting on the ball valve, the ball valve starts to lift out of the seat.

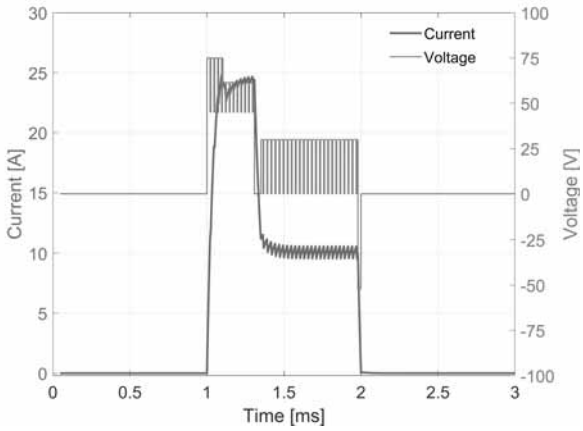

Figure 3: Simulated current- and voltage curve.

Figure 4 shows the actuation current and the valve lift movement of the solenoid valve armature versus time. The negative portion of the valve lift can be attributed to compression and elongation of the components caused by the high system pressure.

The high current in the pull-in phase causes the valve to open quickly.

After a short time, the hold phase begins, during which the ball valve remains open. At the end of actuation, the solenoid valve spring pushes the solenoid armature downwards, closes the valve and thus stops the flow through the outlet throttle.

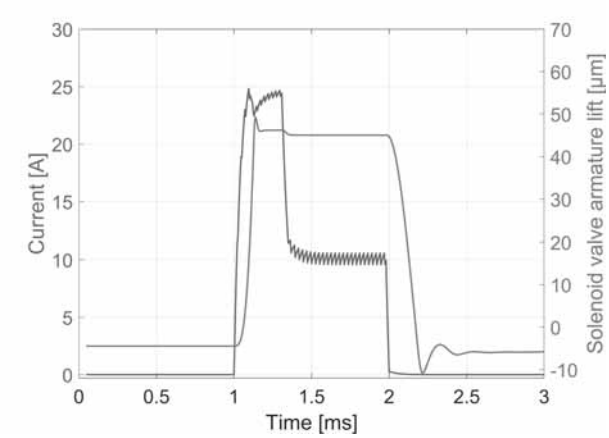

Figure 4: Control current and solenoid valve lift.

1.2 Mechanic-hydraulic Model

This model describes the coupling between the hydraulic and mechanical components in the injector. The lift movement of the solenoid valve armature from the solenoid valve model and a specified fuel pressure are used as input variables.

Figure 5 shows the structure of the injector model in Simscape™. The two hydraulic cylinder blocks represent the nozzle needle and the valve control piston with their corresponding masses.

As in [4], the nozzle holes are modelled by a combination of cross-sectional constriction and a throttling point. In the non-actuated state, the same pressure is present in the control chamber and in the nozzle volume. A force acts on the surface of the control piston and the pressure shoulder of the nozzle needle. Due to the surface ratios, a larger force is created towards the needle seat and the injector remains closed. When the solenoid valve is activated, the ball valve lifts out of the seat and opens the outlet throttle.

As a result, the fuel flows out of the valve control chamber, causing the pressure to drop. So that the pressure difference between the control chamber and the nozzle volume creates a force on the needle in upwards direction causing the needle to open.

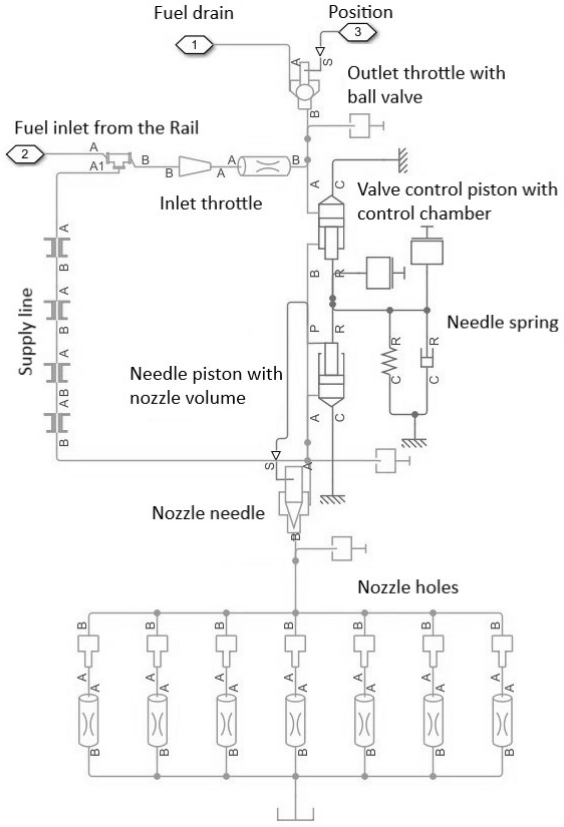

Figure 5: Structure of the injector model in Simscape™.

The opening speed at which the nozzle needle moves depends on the cross-sectional ratio between the inlet and outlet throttle of the control chamber since this ratio influences the resulting pressure in the control chamber.

Figure 6 presents simulation results of the control valve lift, control chamber pressure, needle lift and injection rate for a typical load point revealing the relation of the different parameters. At the end of the solenoid valve actuation, the valve closes the outlet throttle and stops the flow. This causes the pressure in the control chamber to build up, resulting in an increased downward force on the control piston.

The closing speed is largely determined by the inlet throttle. If the hydraulic force from the valve control chamber and the force of the needle spring exceeds the opposing force on the nozzle needle, the nozzle needle begins to close. Injection ends when the nozzle needle reaches the nozzle body seat and closes the nozzle holes.

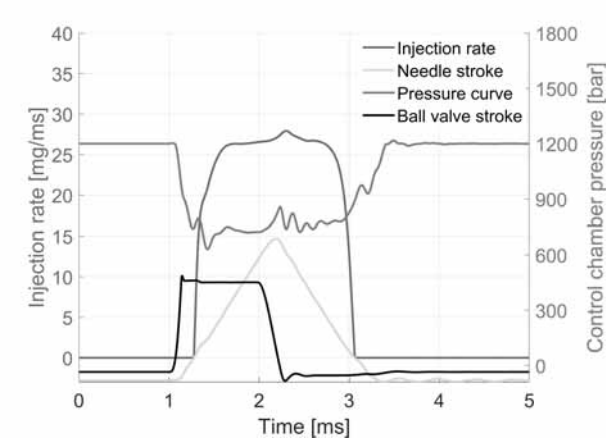

Figure 6: Simulation results injector model.

2 Model Validation

To validate the simulation model, the calculation results are compared with measured data from the injection rate analyser. A comparison of injection rates for two different operating points is shown in Figure 7. In both cases, the measured data curve is the average curve from 150 consecutive injection processes. A comparison of the injection rates shows that the simulation and measurement data are in good agreement. The deviation of the injected quantities between simulation and experiment is around 1%. Similarly good results were also observed at other operating points, which confirms the applicability of the developed injector model.

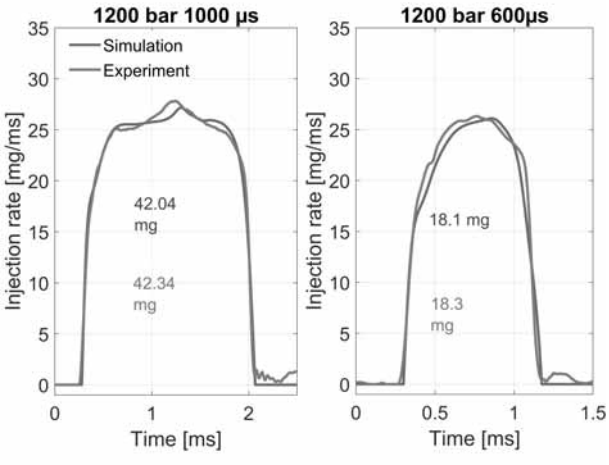

Figure 7: Comparison of injection rates between measurement and simulation at two different injection durations.

3 Combustion Model

The approach presented here describes a global phenomenological combustion model for calculating the heat release rate according to Barba [2].

This model uses the injection rate as an input variable, which opens up more possibilities for parameter studies than conventional empirical models.

As in [6], the basic idea here is that the fuel conversion is controlled by the ignition delay and the fuel vaporisation. The first model component for fuel vaporisation is the calculation of the primary droplet diameter d_{Tr0} [7] according to equation 1.

$$d_{Tr0} = c \cdot d_{D.eff} \cdot (Re \cdot We)^{-0.28} \tag{1}$$

The Reynolds and Weber numbers are calculated using equations 2 and 3.

$$Re = \frac{u_{Tr0} \cdot d_{D.eff}}{\nu_{B.fl}} \tag{2}$$

$$We = \frac{{u_{Tr0}}^2 \cdot d_{D.eff} \cdot \rho_Z}{\sigma_{B.fl}} \tag{3}$$

The output droplet velocity u_{Tr0} is calculated directly from the injection rate according to equation 4.

$$u_{Tr0} = \frac{\frac{dm_E}{dt}}{\rho_{B.fl} \cdot A_{D.eff}} \tag{4}$$

Using the d^2-law in equation 5, the vaporisation time can be calculated for each calculation step based on the output droplet diameter and an empirical factor β.

$${d_{Tr}}^2 = {d_{Tr0}}^2 - \beta \cdot t \tag{5}$$

Literature values for the coefficient c are 8.7 [7], 4.0 [2] and 25.0 [8]. For the vaporisation coefficient β, the value is given as $7 \cdot 10^{-6}$ [2][10]. In addition to the vaporisation time, the ignition delay must also be taken into account.

The ignition delay is generally the time between the start of injection and the first significant release of heat. According to equation 6, Barba [2] divides this into a physical and a chemical component.

$$\tau_{ZV} = \tau_{ZV,phy} + \tau_{ZV,chem} \tag{6}$$

The proportions can be calculated using equations 7 and 8.

$$\tau_{ZV,phy} = c_0 \cdot {u_{Tr0}}^{-1.68} \cdot {d_{D.eff}}^{0.88} \tag{7}$$

$$\tau_{ZV,chem} = c_1 \cdot \left(\frac{p_z}{p_0}\right)^{c_2} \cdot {\lambda_{Zn}}^{c_3} \cdot e^{\frac{T_A}{T_Z}} \tag{8}$$

As the temperatures and pressures change during the calculation of the ignition delay, the ignition integral according to equation 9 is used.

$$1 = \int_{t_{EB}}^{t_{VB}} \frac{1}{\tau_{ZV}}\, dt \tag{9}$$

The ignition event occurs when the integral has reached the value 1. Figure 8 shows the simulation results of the vaporisation model.

The droplet diameter and the corresponding vaporisation time are calculated from the injection rate for each calculation step.

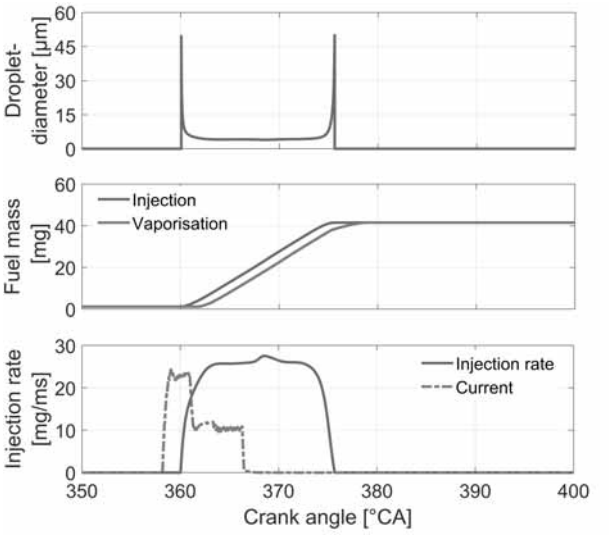

Figure 8: Simulation results vaporisation model.

In Simulink®, the vaporisation time and the ignition delay are transferred to a "Transport Delay" as a time delay. This allows the cumulative injected fuel mass to be shifted by this time period as an input variable.

The most important parameter for the combustion model is the available unburnt mass of vaporized fuel.

The description of diffusion combustion according to equation 10 is based on a frequency approach which, in addition to a characteristic mixing length, also uses a mixing velocity which stands for the turbulence in the combustion chamber [2].

$$\frac{dm_{B.V}}{dt} = \frac{u'}{l_{Diff}} \cdot m_{B.UV} \tag{10}$$

According to equation 11, the mixing length l_{Diff} is made up of the combustion chamber geometry, the current combustion air ratio and the number of nozzle spray holes.

$$l_{Diff} = \sqrt[3]{\frac{V_Z}{\lambda \cdot Anz_D}} \tag{11}$$

Due to the turbulence occurring in the combustion chamber, the mixing velocity u' is divided into a base turbulence and an injection turbulence.

The effects that occur due to inflow or turbulence are recorded in the base turbulence and mapped via the mean piston speed c_m, which represents a rough simplification.

By vectorial addition of the base turbulence and the injection turbulence, equation 12 can be written as follows [2].

$$u' = \sqrt{c_G \cdot {c_m}^2 + c_{Kin} \cdot k} \tag{12}$$

The two parameters c_G and c_{Kin} allow a weighting of the two components as well as an adjustment of the diffusion model to measurement data [2]. Equation 10 can therefore be formulated as follows:

$$\frac{dm_{B.V}}{dt} = \frac{\sqrt{c_G \cdot {c_m}^2 + c_{Kin} \cdot k}}{\sqrt[3]{\frac{V_Z}{\lambda \cdot Anz_D}}} \cdot m_{B.UV} \tag{13}$$

The specific kinetic turbulence energy k summarises the diffusion of the fuel and the kinetic energy supplied to the system as a result of the injection.

This highly simplified $k - l_l$ model is described according to equation 14.

$$\frac{dk}{dt} = -c_{Diss} \cdot \frac{1}{l_l} \cdot k^{\frac{3}{2}} + c_E \cdot \frac{dk_E}{dt} \tag{14}$$

The kinetic energy supplied results from the injection rate over time and the corresponding output droplet velocity.

In addition, Barba takes a global view of the cylinder by using the entire cylinder filling as a scale for the required kinetic energy density [2]. This can be described according to equation 15 as follows:

$$\frac{dk_E}{dt} = \frac{1}{2} \cdot \frac{dm_E}{dt} \cdot {u_{Tr0}}^2 \cdot \frac{1}{m_Z} \tag{15}$$

Using the burnt fuel mass from equation 13 and the lower calorific value for diesel fuel, the heat flux supplied is calculated according to equation 16.

$$\frac{dQ_B}{dt} = H_U \cdot \frac{dm_{B.V}}{dt} \tag{16}$$

For the simulation calculation, this model replaces the previously used combustion model according to Vibe [9] in the energy balance.

Figure 9 shows the comparison of the heat release rate from the pressure curve analysis of experimentally determined measurement data and the phenomenological modelling approach. The second part of the main combustion in particular shows that the phenomenological model delivers a good result. Due to the consideration of the injection rate, the phenomenological model can be used to investigate the impact of further partial injections and variations of hydraulic parameters of the injection system.

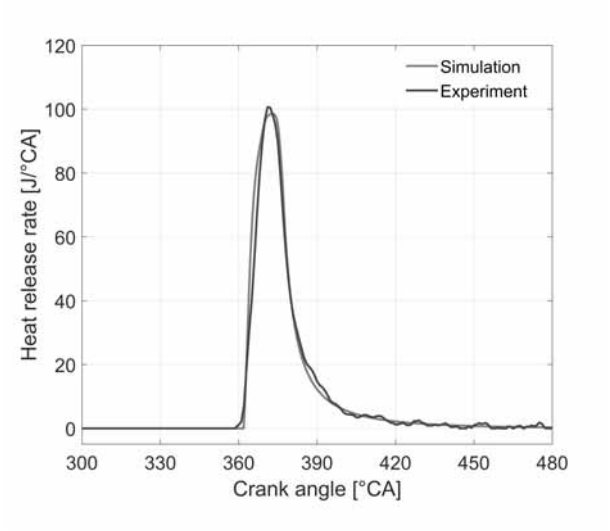

Figure 9: Comparison of heat release rate from cylinder pressure measurement and simulation model.

4 Overall Model Validation

To validate the simulation model, the calculation results are compared with measurement data from the engine test bench. The input parameters such as injector current duration, rail pressure and boost pressure are modelled according to the test bench data.

Figures 10 and 11 show a comparison of the rate of heat release at two different load points. It can be seen that the coupled simulation model shows a high level of agreement with experimentally obtained data even when multiple injection is used.

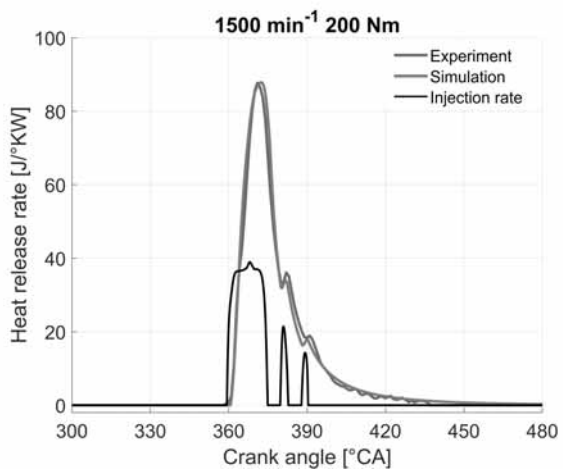

Figure 10: Comparison of the heat release rate determined experimentally and simulatively when using multiple injection at high load

The heat release peaks that occurs after the main injection can clearly be recognised and referred to the post injection events. Further validation is carried out by means of the corresponding cylinder pressure curves at these operating points, which are shown in Figure 12. It can be seen that the combustion behaviour is reproduced very well.

A comparison of the mean pressure, as an integral parameter for characterising the engine load, shows a deviation of 2 % between measurement and simulation. Similarly, good results were also observed at other operating points with single and multiple injection, which confirms the applicability of the simulation approach and the selected models.

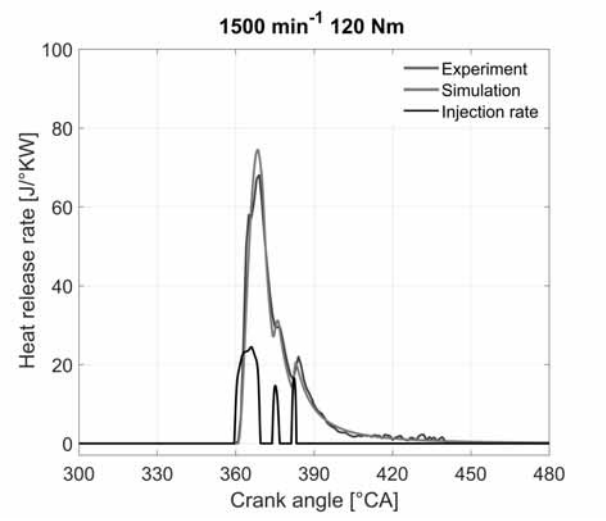

Figure 11: Comparison of the heat release rate determined experimentally and simulatively when using multiple injection at medium load.

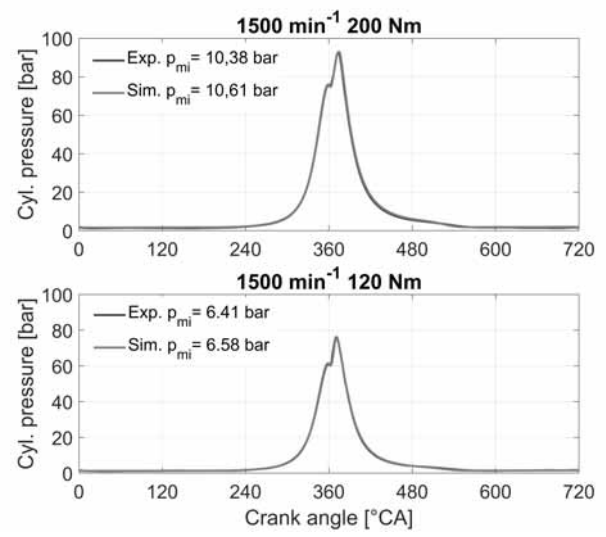

Figure 12: Comparsion of the cylinder pressure curve between simulation and measurement for two different load points.

5 Conclusion and Outlook

The modelling approach presented in this article describes a 1D hydraulic injector model in Simscape™, which was coupled with a phenomenolgical combustion model implemented in Simulink®. The injector model is a powerful tool which allows for a detailled description of the injector behaviour.

The combustion model provides a very good basis for calculating the heat release in the combustion chamber considering the injection rate. A comparison of the simulation results showed very good agreement with the measurement results from the engine test bench, which supports the applicability of these modelling approaches.

A key objective for future work is the further development of the model with regard to dynamic operating scenarios. Furthermore, a focus is on implementing a nitric oxide emission model in order to analyse the emission behaviour in parameter studies and to derive optimisation measures.

Acknowledgement

The results presented here were obtained within the framework of the publicly funded project SIDYN (FKZ:13FH043PX8) and the doctoral program of Wismar University of Applied Sciences.

The authors want to thank the BMBF and Wismar University for the provided financial support.

Nomenclature

β - vaporisation coefficent [m^2/s]
λ - air fuel ratio [-]
λ_{Zn} - local air fuel ratio [-]
$\nu_{B.fl}$ - liquid fuel viscosity [m^2/s]
$\rho_{B.fl}$ - liquid fuel density [kg/m^3]
ρ_Z - density in the combustion chamber [kg/m^3]
$\sigma_{B.fl}$ - liquid surface tension [N/m]
τ - time [s]
τ_{ZV} - ignition delay [s]
$A_{D.eff}$ - effective nozzle cross-section [mm^2]
c - universal constant [-]
c_m - mean piston speed [m/s]
$d_{D.eff}$ - effective nozzle diameter [mm]
H_U - lower calorific value [J/kg]
k - specific kinetic turbulence energy [m^2/s^2]
l_{Diff} - mixing length [m]
l_l - length scale [m]
m_B - fuel mass [kg]
m_E - injected fuel mass [kg]
p_0 - ambient pressure [bar]
p_{mi} - indicated medium pressure [bar]
p_z - cylinder pressure [bar]
Q_B - energy released during combustion [J]
Re - Reynolds number [-]
T_A - activation temperature [K]
t_{EB} - start of injection [s]
t_{VB} - start of combustion [s]
T_Z - gas temperature in the combustion chamber [K]
u' - turbulence intensity [m/s]
u_{Tr0} - output droplet velocity [m/s]
V_Z - cylinder volume [m^3]
We - Weber number [-]

References

[1] Jörss, D., Herrmann, B., Fink, C. *Modellierung des Betriebsverhaltens eines Diesel-Industriemotors als Stromerzeuger*, Virtueller ASIM Workshop der Fachgruppe STS/GMMS & EDU, 2021, DOI: 10.11128/arep.45

[2] Barba, C. *Erarbeitung von Verbrennungskennwerten aus Indizierdaten zur verbesserten Prognose und rechnerischen Simulation des Verbrennungsablaufes bei Pkw-DE-Dieselmotoren mit Common-Rail-Einspritzung*, Zürich, ETH Zürich, Diss., 2001.

[3] Audi AG, *http://www.volkspage.net/technik/ssp/ssp/SSP_227.PDF*, letzter Zugriff: 08.12.2022

[4] Vermeiden, J.C. *Fuel injection equipment characterisation for short and multiple injections experimental setup design and model-based sensitivity analysis* , Eindhoven University of Technology, 2020.

[5] Payri, R., Salvador, FJ., Carreres, M., De la Morena, J. *Fuel temperature influence on the performance of a last generation common-rail diesel ballistic injector. part ii: 1d model development, validation and analysis* Energy Conversion and Management, 114:376-391, 2016.

[6] Constien, M., R., Woschni G. *Vorausberechnung des Brennverlaufes aus dem Einspritzverlauf für einen direkteinspritzenden Dieselmotor*, MTZ 53, Nr.7/8, 1992.

[7] Varde, K.S., Popa, D.M., Varde L.K. *Spray Angle and Atomization in Diesel Sprays*, SAE 841055, 1984.

[8] Kožuch, P. *Ein phänomenologisches Modell zur kombinierten Stickoxid- und Rußberechnung bei direkteinspritzenden Dieselmotoren*, Stuttgart, Universität Stuttgart, Diss., 2004.

[9] Vibe, I. *Brennverlauf und Kreisprozess von Verbrennungsmotoren*, VEB Verlag Technik, Berlin, 1970.

[10] Grill, M. *Objektorientierte Prozessrechnung von Verbrennungsmotoren*, Stuttgart, Universität Stuttgart, Diss., 2006.